Bioactive Materials 26 (2023) 128–141

Contents lists available at ScienceDirect

Bioactive Materials

journal homepage: www.keaipublishing.com/en/journals/bioactive-materials

Degradation behavior of ZE21C magnesium alloy suture anchors and their effect on ligament-bone junction repair

Delin Ma [a], Jun Wang [a,b,c,*], Mingran Zheng [a], Yuan Zhang [a], Junfei Huang [d], Wenxiang Li [e], Yiwen Ding [a], Yunhao Zhang [a], Shijie Zhu [a,b,c], Liguo Wang [a,b,c], Xiaochao Wu [a,b,c], Shaokang Guan [a,b,c,**]

[a] School of Material Science and Engineering, Zhengzhou University, Zhengzhou, 450001, China
[b] Henan Key Laboratory of Advanced Magnesium Alloys, Zhengzhou, 450002, China
[c] Key Laboratory of Advanced Materials Processing & Mold, Ministry of Education, Zhengzhou, 450002, China
[d] Shimadzu (China) Co., Ltd, Shenzhen Branch, Shenzhen, 528042, China
[e] Zhengzhou Orthopedic Hospital, Zhengzhou, 450053, China

ARTICLE INFO

Keywords:
ZE21C
Suture anchor
Degradation behavior
Reparative effect
Ligament-bone junction

ABSTRACT

Current materials comprising suture anchors used to reconstruct ligament-bone junctions still have limitation in biocompatibility, degradability or mechanical properties. Magnesium alloys are potential bone implant materials, and Mg^{2+} has been shown to promote ligament-bone healing. Here, we used Mg-2 wt.% Zn-0.5 wt.% Y-1 wt.% Nd-0.5 wt.% Zr (ZE21C) alloy and Ti6Al4V (TC4) alloy to prepare suture anchors to reconstruct the patellar ligament-tibia in SD rats. We studied the degradation behavior of the ZE21C suture anchor via *in vitro* and *in vivo* experiments and assessed its reparative effect on the ligament-bone junction. *In vitro*, the ZE21C suture anchor degraded gradually, and calcium and phosphorus products accumulated on its surface during degradation. *In vivo*, the ZE21C suture anchor could maintain its mechanical integrity within 12 weeks of implantation in rats. The tail of the ZE21C suture anchor in high stress concentration degraded rapidly during the early implantation stage (0–4weeks), while bone healing accelerated the degradation of the anchor head in the late implantation stage (4–12weeks). Radiological, histological, and biomechanical assays indicated that the ZE21C suture anchor promoted bone healing above the suture anchor and fibrocartilaginous interface regeneration in the ligament-bone junction, leading to better biomechanical strength than the TC4 group. Hence, this study provides a basis for further research on the clinical application of degradable magnesium alloy suture anchors.

1. Introduction

Tendon and ligament injuries account for more than 30% of musculoskeletal diseases, with more than 4 million new cases worldwide every year [1], causing a severe burden on society and economies [2]. Mild tendon and ligament injuries can usually be relieved quickly after proper treatment by professional doctors. The main feature of severe soft tissue injury is that the end of the tendon/ligament and the bone surface can be broken due to low strength, such as rotator cuff tears, ankle collateral ligament injuries and elbow soft tissue injuries. Suture anchors are the commonly used fixation implants for these types of injuries [3]. The therapeutic mechanism is placing suture anchors under the cortical bone and attaching tendons or ligaments to bone through sutures to maintain tendons-bone or ligaments-bone without loosening until healing [4,5].

After more than 30 years of development, standard guidelines for preparing clinical suture anchors have concluded. These include: maximizing pull-out strength, minimizing acute iatrogenic injury, and preventing long-term applications to minimize the possibility of developing arthritis [6]. These factors are closely related to the material and structure of the anchor itself [7,8]. The most commonly used suture anchor materials include non-degradable titanium alloys, stainless steel, PEEK and degradable polymer materials [9]. However, there were limitations in their clinical application. The titanium alloys and stainless

Peer review under responsibility of KeAi Communications Co., Ltd.
* Corresponding author. School of Material Science and Engineering, Zhengzhou University, Zhengzhou, 450001, China.
** Corresponding author. School of Material Science and Engineering, Zhengzhou University, Zhengzhou, 450001, China.
E-mail addresses: wangj@zzu.edu.cn (J. Wang), skguan@zzu.edu.cn (S. Guan).

https://doi.org/10.1016/j.bioactmat.2023.02.021
Received 21 October 2022; Received in revised form 18 February 2023; Accepted 18 February 2023

steel are prone to the stress shielding effect, and their long-term implantation causes osteolysis [10]. The biological inertness of PEEK limits osseointegration and its weak antibacterial property will lead to the formation of perianchor cyst [11,12]. The degradable polymer materials have poor mechanical properties and accumulate acidic products during the degradation process, leading to complications such as effusion, cyst formation and arthritis [13,14]. Therefore, it is necessary to use new materials with better performance and biocompatibility to prepare suture anchor.

Magnesium is a biodegradable metal with good biocompatibility and Young's modulus close to that of natural cortical bone. Moreover, its harmless degradation products can be excreted via normal human metabolism, so it is widely regarded as a potentially revolutionary bone implant material [15,16]. Moreover, with the continuous research on the magnesium-based bone implants, it was found that the Mg^{2+} released by magnesium-based bone implants have beneficial effects on bone tissue and bone-ligament/tendon interface healing [17–19]. Therefore, the Mg-based suture anchor has great application potential. However, the rapid degradation rate of magnesium-based implants and the detrimental effects of hydrogen generation on the recovery of bone tissue have limited the use of magnesium in orthopedic applications [20,21].

The addition of alloying elements and the optimization of the alloy production process can improve the corrosion resistance of magnesium alloys and slow down their hydrogen release rate [22–24]. In this study, we used the previously reported Mg-2 wt.% Zn-0.5 wt.% Y-1wt.% Nd-0.5 wt.% Zr alloy (hereafter denoted as the ZE21C alloy) that overcame the problems of cytotoxicity and excessive corrosion rate [25] and used the widely clinical suture anchor material Ti6Al4V (hereafter denoted as the TC4 alloy) as a control group to prepare suture anchors. The reconstruction of the patellar ligament-tibia surgery of SD rats within 12 weeks was performed using the ZE21C or TC4 suture anchors. The degradation behavior of the ZE21C suture anchor was evaluated via *in vitro* and *in vivo* experiments, and its reparative effect on ligament-bone junction was evaluated through radiological, histological and biomechanical assays. We hypothesized that the ZE21C magnesium alloy suture anchor could maintain its mechanical integrity within 12 weeks and promote ligament-bone healing.

2. Materials and methods

2.1. Material and sample preparation

2.1.1. Alloy praparation

High-purity magnesium (99.99 wt.%) ingots, high-purity zinc (99.99 wt.%) ingots, Mg-28.5 wt.% Y master alloy, Mg-30 wt.% Nd master alloy, and Mg-30 wt.% Zr master alloy were selected as raw materials. The alloy ingots were prepared by permanent mold casting at a pouring temperature of 720 °C and air cooling. The as-cast billets of the alloys were annealed at 370 °C for 24 h, following by furnace cooling. Finally, the annealed alloy samples were hot extruded directly into bars at 320 °C with an extrusion speed and extrusion ratio of 2 mm/min and 36, respectively. The actual composition (Table 1) and mechanical properties of the ZE21C rods were tested using inductively coupled plasma mass spectrometry and a universal testing machine to ensure that the performance of the rods meet the requirements.

2.1.2. Suture anchors praparation

Qualified ZE21C magnesium alloy extruded rods and TC4 titanium alloy rods (commercial standard, Taizhou Daoguan Rubber & Plastic Products Co., Ltd., China) were used to manufacture the designed suture anchors on a CNC lathe (SB-ZOR, STAR Precision Co., Ltd., Japan). Accroding to the ASTM F543-17 to test the pull-out strength, ZE21C suture anchor is 130.30 ± 7.24 N and TC4 suture anchor is 118.79 ± 6.87 N. All suture anchors were ultrasonically cleaned in absolute ethanol, sterilized with 25 kGy of ^{60}Co radiation, and vacuum-packed. All suture anchors were designed similarly and were deemed to be suitable for use in rats. The outer diameters and lengths of the suture anchors were fixed at 2.6 mm and 5.5 mm. The details of the suture anchor are shown in Fig. 1.

2.2. In vitro corrosion experiments

The *in vitro* corrosion experiment was carried out in Hanks' solution, and the ratio of solution volume to the sample area was set to 20 mL/cm^2 according to the ASTM-G31-72 standard. The centrifuge tube was placed in a constant temperature water bath at 37 °C, and the Hanks' solution was replaced daily. Samples were taken from the Hanks' solution after 1, 4, 7, and 14 days, using three parallel samples per test point. And during the 14 days soaking process, the pH value of the solution was recorded at the same time every day before changing the Hanks' solution. The removed samples were rinsed with deionized water and dried in an oven at 37 °C. SEM and EDS (Scanning electron microscopy, Philips Quanta-200, Japan) were used to characterize their surfaces and corrosion products. To calculate the *in vitro* degradation rate, the samples were cleaned with a chemical reagent containing 2g Cr_2O_3, 1g $AgNO_3$, and 100 g H_2O. The products were dried in a drying oven at 37 °C for 6 h. The vitro degradation rate (DR_{vitro}) was calculated according to ASTM-G 31-72 standard using equation (1) as follows:

$$DR_{vitro} = \Delta W / (A \times T \times \rho) \quad (1)$$

where ΔW (g) is the mass loss (accurate to 1 mg), A (cm^2) is the surface area (accurate to 0.01 cm^2), T (year) is the soaking time, and ρ (g/cm^3) is the density of the immersion material.

2.3. Finite element model

The tibias of male SD rats weighing 300 g were selected for continuous axial tomography using an SMX-225CT system (Shimadzu Company, Japan). A total of 1718 layers of DICOM data were obtained under scanning conditions of 200 kV of voltage and a 70 mA current. DICOM format data were successively imported into Mimics Medical 20.0 software for modeling and Geomagic Wrap for optimization and smoothing. Finally, tibia geometric models were obtained, as shown in Fig. 2a. The suture anchor and tibia models (Fig. 2b) were imported into Solidwork2018 software to assemble the suture anchor implant (Fig. 2c). The 3D geometrical model of the assembly was imported into Ansys software for finite element analysis.

The element type of the model was a 4-node entity model. The total number of nodes and elements were 87,988 and 60,483, respectively, as shown in Fig. 2d. The force conditions were set as follows: the force applied to the proximal tibia was 2 N, the suture anchor received a normal tension of 10 N, and the tibia bottom was fixed to evaluate the mechanical response of the suture anchor, as shown in Fig. 2e. The tibia and suture anchors were set as isotropic, uniform, and continuous linear elastic materials. The related attributes for materials were defined from previous studies [26,27] (Table 2).

Table 1
The actual composition of ZE21C magnesium alloy.

Actual composition	Zn	Y	Nd	Zr	Ni	Cu	Fe	Mg
ZE21C	2.3	0.51	1.2	0.63	<0.001	<0.001	<0.001	Bar

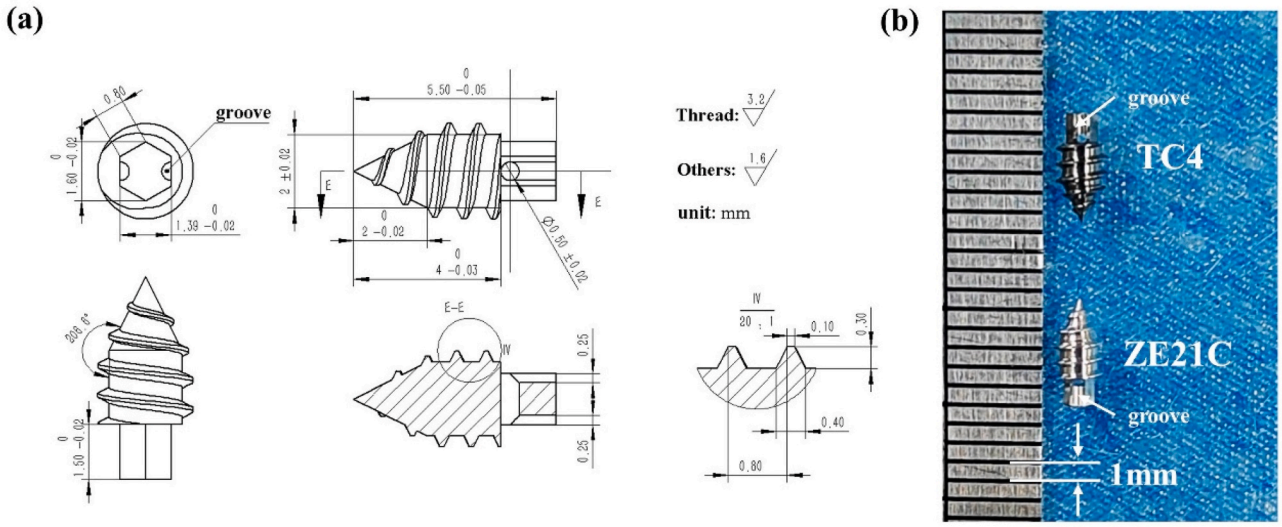

Fig. 1. Design of the suture anchor (a) and the resulting products (b).

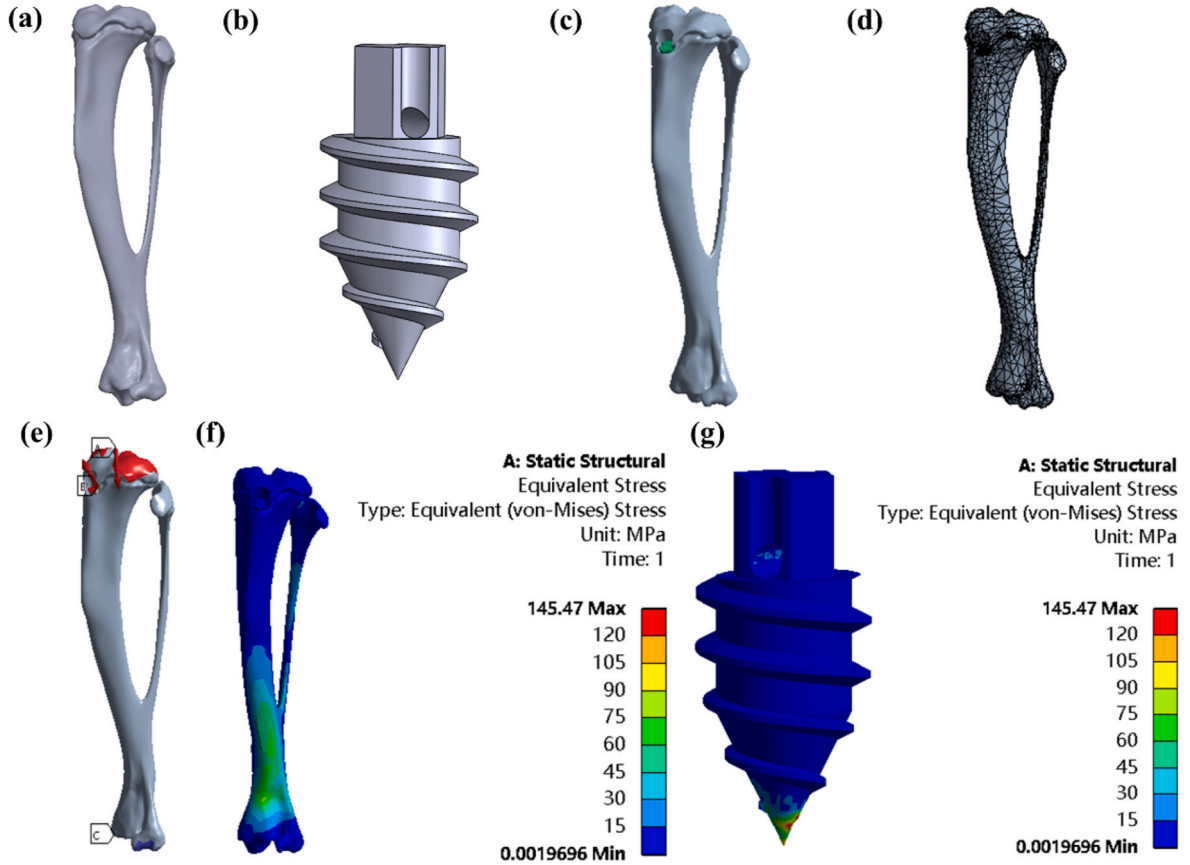

Fig. 2. (a) Geometric model of the rat tibia. (b) Geometric model of the suture anchor. (c) Geometric model of the assembly. (d) Mesh model of the assembly. (e) Condition settings: A, the force applied to the proximal tibia; B, normal tension; and C, fixation. (f) Stress on the rat tibia. (g) Stress on the suture anchor.

2.4. In vivo experiments

2.4.1. Animal patellar ligament-tibia reconstruction model

Forty-eight nine-week-old male SD rats weighing 280–320 g were used to establish the patellar ligament-proximal tibia reconstruction model. The study protocol was approved by the Ethics Committee of the Animal Experimental Center of Zhengzhou University (reference number: SYXK(Yu)2020-0008). The entire surgical process strictly adhered to aseptic principles. The skin and subcutaneous tissue of the rats (about 20 mm) were incised longitudinally along the knee joint to fully expose the shape of the patellar ligament. Damage to the patellar ligament was done using a scalpel against the bone surface of the patellar ligament and the tibia joint to cut off the attachment point. Using a medical bone drill, a 1.2-mm-diameter bone hole was drilled at the proximal tibial attachment point along the front of the tibia. Then, a suture anchor was screwed along the hole, and a clinical PGA suture (Shanghai Jinhuan

Table 2
Material properties of the rat tibia and ZE21C suture anchor.

Model	Density (g/cm^3)	Yield strength (MPa)	Ultimate Strength (MPa)	Young's modulus (GPa)	Poisson's ration
Rat tibia	1	115	130	20	0.3
ZE21C suture anchor	1.74	275	345	45	0.3

Medical Supplies Co., Ltd., China) was used to fix the patellar ligament to the original attachment point. The internal ligament and external skin were then sewn using sterile sutures and disinfected by wiping with iodine. The surgical process is shown in Fig. 3. SD rats were housed individually in cages and allowed to move freely after surgery. Subcutaneous injection of penicillin sodium (15 mg/kg body weight) was performed three consecutive days after the operation. Finally, the rats were sacrificed at 2, 4, 8, and 12 weeks postoperatively for follow-up studies.

2.4.2. X-ray examination

X-ray scanning was performed on the lateral surface of the right tibia of the rats at 1 day and 2, 4, 8, and 12 weeks post-implantation to observe the position of the suture anchor and the morphological changes of the implantation site, such as bone formation or generation of gas.

2.4.3. Determining the range of motion (ROM) of the knee

At 2, 4, 8, and 12 weeks after surgery, the ROM of the rat knee was measured under anesthesia. The range of motion was measured via three-point positioning using a protractor. The three points were respectively set at the proximal femur near the joint, the lateral femoral condyle, and the lateral malleolus of the distal tibia, and the angles corresponding to the maximum ROM of the knee joint were measured. Measurement was performed by the same person. During the operation, measurements were taken from the same rat three times in a blinded manner, and the average values were calculated.

2.4.4. Micro-CT examination

At 2, 4, 8, and 12 weeks after surgery, three patellar ligament-tibial complexes (PLTs) from each group of rats were collected for Micro-CT scanning to evaluate the *in vivo* degradation of ZE21C suture anchors and new bone formation above the suture anchor. The settings of the Micro-CT device (SMX-225CT, Shimadzu, Japan) were as follows: 115 kV and 70 μA in the X-ray tube; scanning resolution, 15 μm; and exposure time, 1000 ms. The degradation rate was calculated from the volume change of the reconstructed ZE21C suture anchor. The vivo degradation rate (DR_{vivo}) was calculated using equation (2) as follows:

$$DR_{vivo} = \Delta V / (A \times T) \quad (2)$$

where ΔV (mm^3) is the volume loss, accurate to 0.01 mm^3; A (mm^2) is the surface area, accurate to 0.01 mm^2; and T (year) is the implantation time.

Furthermore, a cylindrical area of bone with a diameter of 2 mm and a height of 1.5 mm above the suture anchor was designated as the region of interest (ROI). Furthermore, VGSTUDIO MAX was used to calculate the trabecular parameters of ROI, including the bone volume over total volume (BV/TV), trabecular number (Tb. N), trabecular thickness (Tb. Th) and trabecular separation (Tb. Sp).

2.4.5. Histological procedure

Each whole PLTs was fixed in a 4% paraformaldehyde solution for 24 h. Afterward, the suture anchors were removed from the direction opposite the implant, avoiding damaging the tissue above the suture anchor. The rest of the PLTs were rapidly decalcified using an EDTA decalcification solution (Servicebio, China) for one week before histological processing. The specimens were then dehydrated with a graded ethanol series (Sinopharm Chemical Reagent, China), cleared with xylene (Sinopharm Chemical Reagent, China), and embedded in paraffin for histological examination. Sagittal sections at the suture anchor insertion area were cut to a thickness of 5 μm and stained with hematoxylin and eosin (HE), safranin O and fast green, and toluidine blue. Individual sections from each sample were analyzed.

PLTs with suture anchors were fixed in 4% paraformaldehyde for 48h. After sequential dehydration in 50%, 75%, 85%, 95% and 100% ethanol, PLTs were embedded in polymethylmethacrylate. The resin block embedded with the PLTs was polished to the maximum cross section of the suture anchor for subsequent SEM&EDS observation.

2.4.6. Suture anchors in vivo and bone-implant interface analysis

SEM/EDS analysis was performed to observe the morphology of the

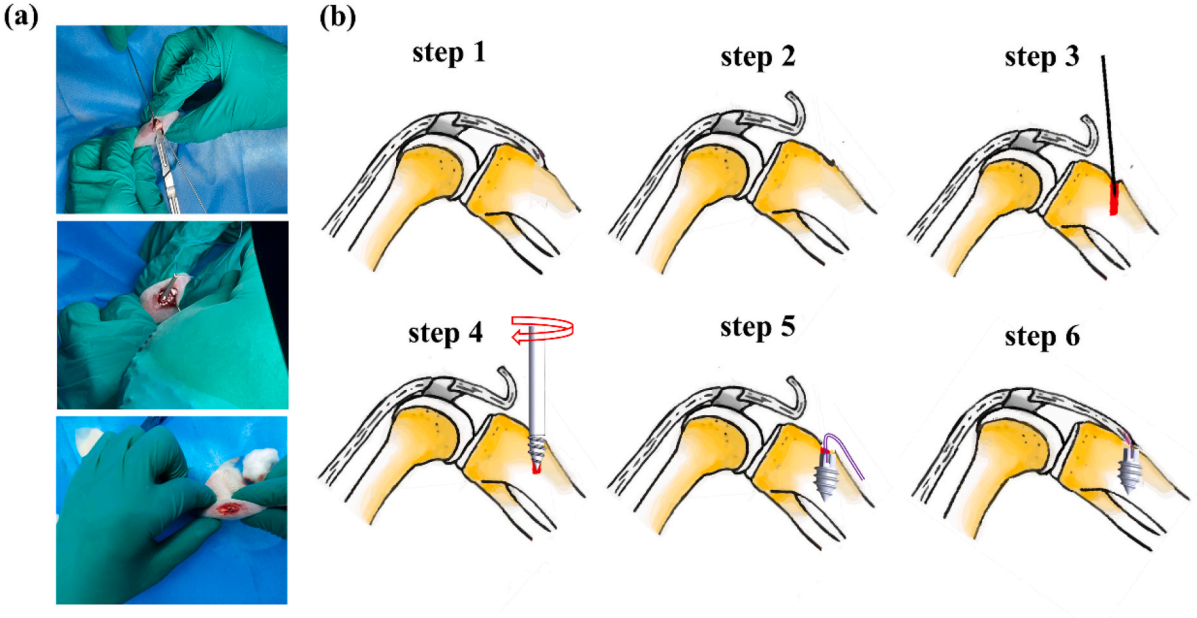

Fig. 3. The surgical procedure (a) and schematic diagram (b) of the patellar ligament-tibia reconstruction process in SD rats.

removed suture anchors (SEM, Philips Quanta-200, Japan) and to analysis the bone-implant interface on the cross section of the resin block embedded with the PLTs (SEM, Helios G4 CX, USA).

2.4.7. Blood indices analysis

Blood samples were collected from the abdominal venous blood between two groups of rats at 12 weeks after surgery. Whole blood metallic elements of Mg, Zn, Y, Nd and Zr were measured by ICP-MS. Liver function was evaluated by aspartate aminotransferase and serum albumin levels, while kidney function was evaluated by serum creatinine and Urea nitrogen levels using the automatic biochemical analyzer (BS-240VET, China).

2.4.8. Biomechanical testing

Three PLTs in each group were collected at 2, 4, 8, and 12 weeks after surgery and stored in a low-temperature device at 40 °C for biomechanical testing to evaluate the healing quality at the ligament-bone repair site. The PLTs were thawed overnight at 4 °C and moistened with saline before the start of the experiment to prevent tissue dehydration. The patellar ligament and tibia were fixed on a tensile test fixture customized for the tensile machine (ZQ990B, China), the axial direction of the sample was ensured to be parallel, and a constant tensile load of 1 N was applied. The width and thickness of the proximal tibia patellar ligament were measured with a caliper to calculate the tensile strength. A 2 kN test sensor was used to record the tensile load, and a load was applied at a displacement rate of 10 mm/min until the final failure load of the patellar ligament. A load-displacement curve was generated, and the ultimate failure load, tensile strength and stiffness were calculated.

2.5. Statistical analysis

The results were analyzed using one-way ANOVA with Tukey's post hoc test in SPSS 17.0 software (SPSS Inc. Chicago, IL). Differences were considered statistically significant at $p < 0.05$. *, **, and *** indicate significance levels of $p < 0.05$, $p < 0.01$, and $p < 0.001$, respectively.

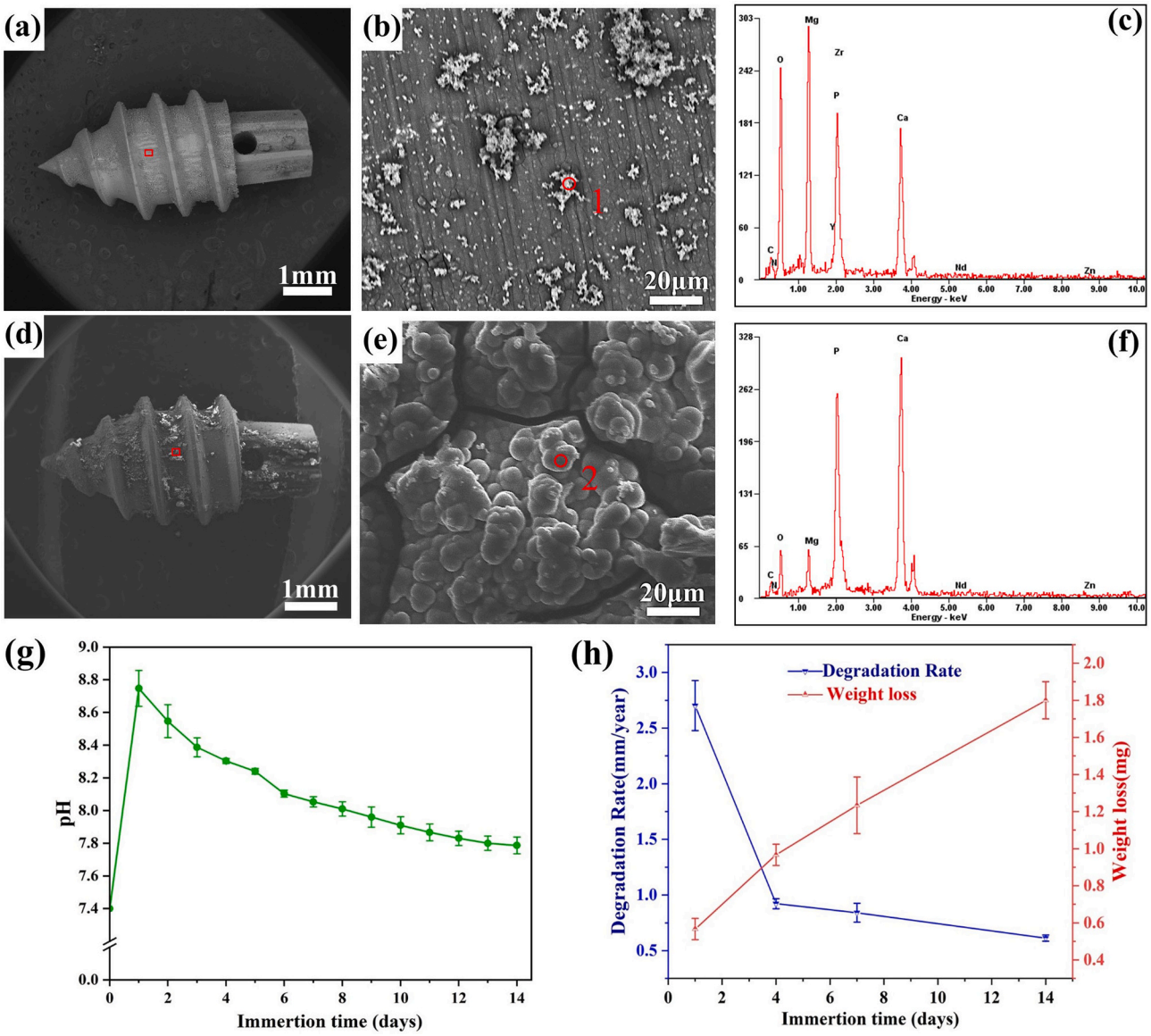

Fig. 4. Surface morphology and EDS measurements of the ZE21C suture anchors immersed in Hanks' solution. (a) Surface morphology after one day, (b) after one day (magnification, 1000 ×), and (c) EDS of point 1. (d) Surface morphology after 14 days, (e) after 14 days (magnification, 1000 ×), and (f) EDS of point 2. (g) pH changes during 14 days of immersion in Hanks' solution. (h) weight loss and *in vitro* degradation rate curves.

3. Results

3.1. In vitro degradation of the ZE21C suture anchor

ZE21C suture anchors degraded over time after soaking in Hanks' solution. After soaking for one day, the ZE21C suture anchor was covered with flocculent material on the whole surface (Fig. 4a). Microscopic cracks and aggregated microcrystalline products were observed on the surface of the suture anchors (Fig. 4b), suggesting ZE21C suture anchor degraded gradually due to galvanic corrosion. After soaking for 14 days, the amount of flocculent products on the surface of the ZE21C suture anchor increased significantly (Fig. 4d). Microscopically, many spherical products were observed on the surface of the anchors, and there were deep cracks surrounding them (Fig. 4e). Compared with soaking for one day, the proportion of Ca and P elements in the products soaked for 14 days was significantly increased (Fig. 4c and f). Some studies have shown that the accumulation of Ca and P products can help promote bone formation and delay the degradation of magnesium alloys [28].

The pH changes during immersion were recorded in Fig. 4g, showing that the pH of the ZE21C anchor gradually decreased and reached to 7.79 ± 0.05 after soaking for 14 days. It indicated that the OH^- ion generation rate from the degradation of ZE21C suture anchors gradually weakened over time. The mass loss during immersion and the calculated degradation rate were recorded in Fig. 4h, which showed that the degradation rate of the ZE21C suture anchor continued to decrease over time at a calculated degradation rate of 0.61 ± 0.03 mm/year after 14 days.

3.2. Finite element simulations

As shown in Fig. 2f-g, the simulation results showed that the stress in the tibia was mainly concentrated at the root, with a magnitude of approximately 45–75 MPa. It was also observed that a small amount of stress was concentrated in the hole of the ZE21C suture anchor, with a magnitude of approximately 15-30 MPa. The other stress concentration was mainly located at the tail of the anchor, with a magnitude of approximately 75 MPa. The maximum stress was 145.47 MPa.

3.3. X-ray imaging examination

Compared with the TC4 group, a small shadow appeared above the implantation site in the ZE21C group one day after surgery, which may be the subcutaneous emphysema caused by the degradation of the magnesium alloy. Two weeks after the operation, the gas shadow was transferred to the surroundings of the ZE21C suture anchor. Four weeks post-operation, the gas shadow area still existed, but its size was relatively reduced. At 8 and 12 weeks after the operation, the gas shadow around the ZE21C suture anchor disappeared, the volume of the magnesium alloy anchor gradually decreased, and the surrounding bone density gradually approached average bone density (Fig. 5). Neither group showed any sign of suture anchor dislocation throughout the experiment.

3.4. In vivo degradation behavior of ZE21C suture anchors

According to the three-dimensional morphology of the ZE21C suture anchor extracted via Micro-CT analysis, it was observed that the suture anchor gradually degraded over time (Fig. 6a). Although there was local degradation at the head of the anchor, the anchor maintained its overall structure at 12 weeks post-implantation. As shown in Fig. 6b, the anchors degraded rapidly in the first four weeks post-implantation, with a degradation rate ranging from 0.5 to 0.7 mm/year, gradually slowing down after that. At 12 weeks of implantation, the degradation rate was 0.30 ± 0.01 mm/year, and the remaining volume was about 75% of the original. As shown in Fig. 6c, the head, middle and tail of the suture anchor were divided into parts I, II, and III, respectively, and the residual volume was calculated. After 2 weeks of implantation, the degradation of part I was the slowest, with a residual volume percentage of 94.14 ± 1.62%, followed by part II, whose residual volume percentage was 92.12 ± 0.68%, while that of part III was 85.10 ± 2.09%. With an increase in implantation time, the degradation of part I was accelerated, and its residual volume percentage was lower than the overall average, while the degradation of part II remained uniform. The degradation of part III gradually slowed down, and its final residual volume percentage became close to that of part I. Fig. 6d shows the representative SEM morphologies of the ZE21C suture anchors at 2, 4, 8, and 12 weeks post-

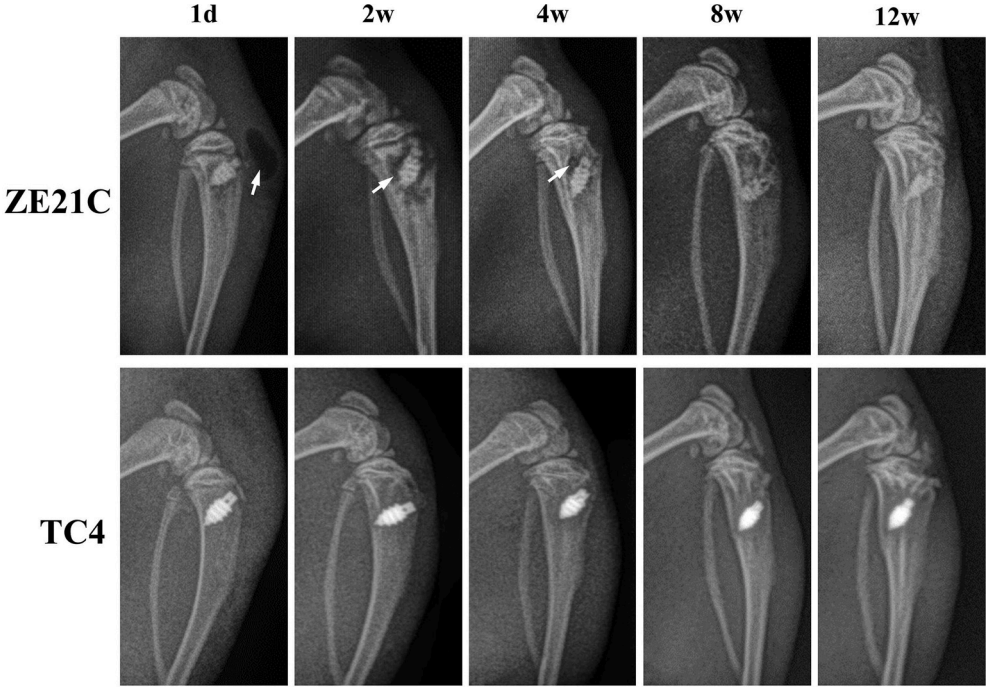

Fig. 5. Representative radiographic images at 1 day, and 2, 4, 8, and 12 weeks after implantation. White arrows: gas shadow.

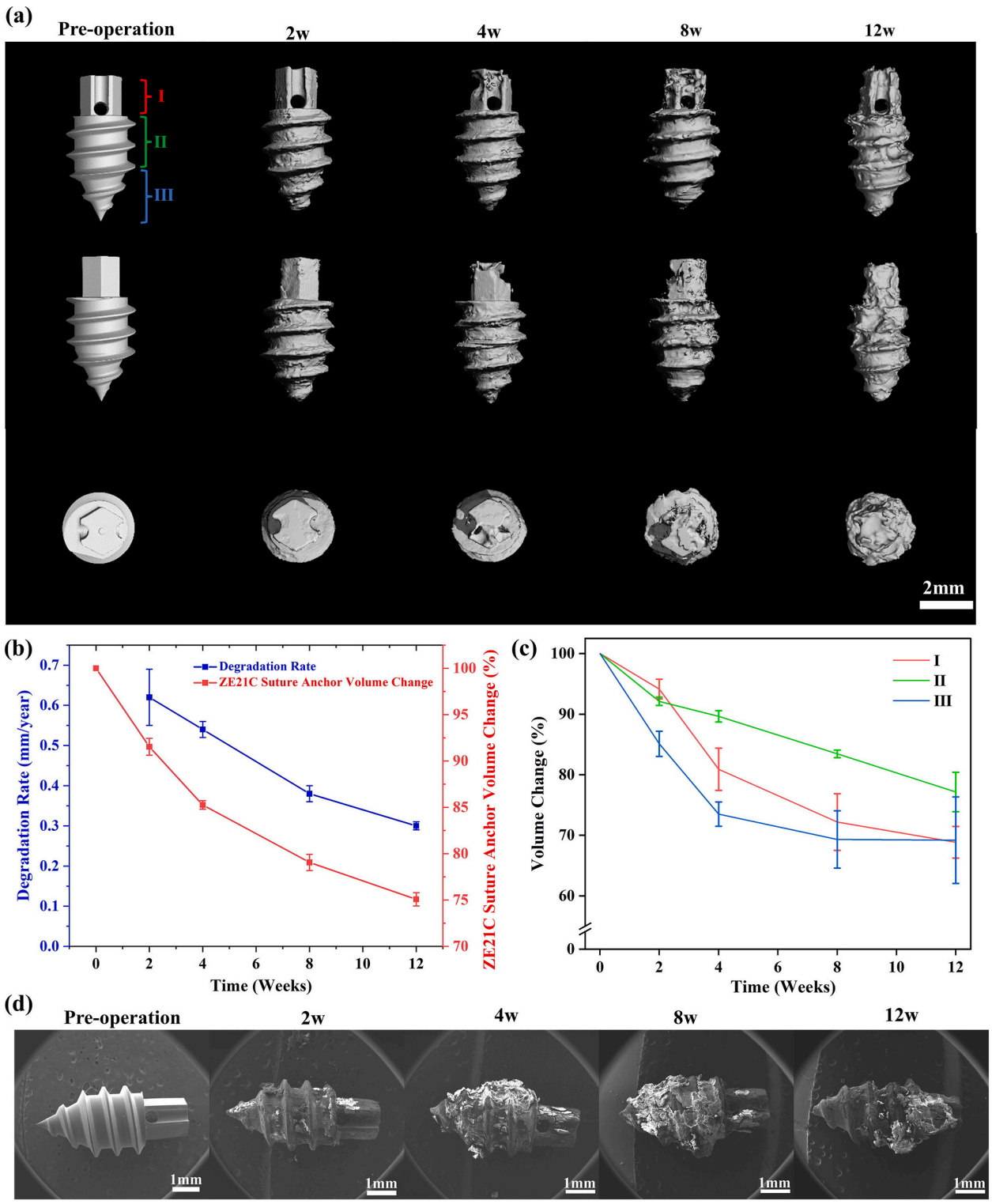

Fig. 6. (a) 3D Micro-CT images of the implanted ZE21C suture anchor. (b) Volume change and vivo degradation rate of ZE21C suture anchor at 2, 4, 8, and 12 weeks post-implantation. (c) Volume change of part I, II and III for ZE21C suture anchor. (d) SEM morphologies of the ZE21C suture anchor after 0, 2, 4, 8, and 12 weeks post-implantation.

operation. It can be observed that the surface of the ZE21C suture anchor are gradually covered by the surrounding tissue, indicating that the ZE21C magnesium alloy has good biocompatibility.

As shown in Fig. 7a and c, at two weeks post-implantation, the sharp part of the ZE21C suture anchor thread was preferentially corroded, and the surrounding bone tissue attachment area was significantly more than that of the TC4 group. After 12 weeks post-implantation, the threads of the ZE21C and TC4 suture anchors were covered by bone tissue (Fig. 7b and d). However, by observing the element distribution of bone-implant interface (Fig. 7e), these was gap filled with resin in the interface of TC4 suture anchor and bone, where the C content was high, while the Ca and P content was low. In contrast, the elemental content in the degraded layer of the ZE21C anchor thread was similar to that of the surrounding bone tissue (Fig. 7f). These results indicated that the ZE21C

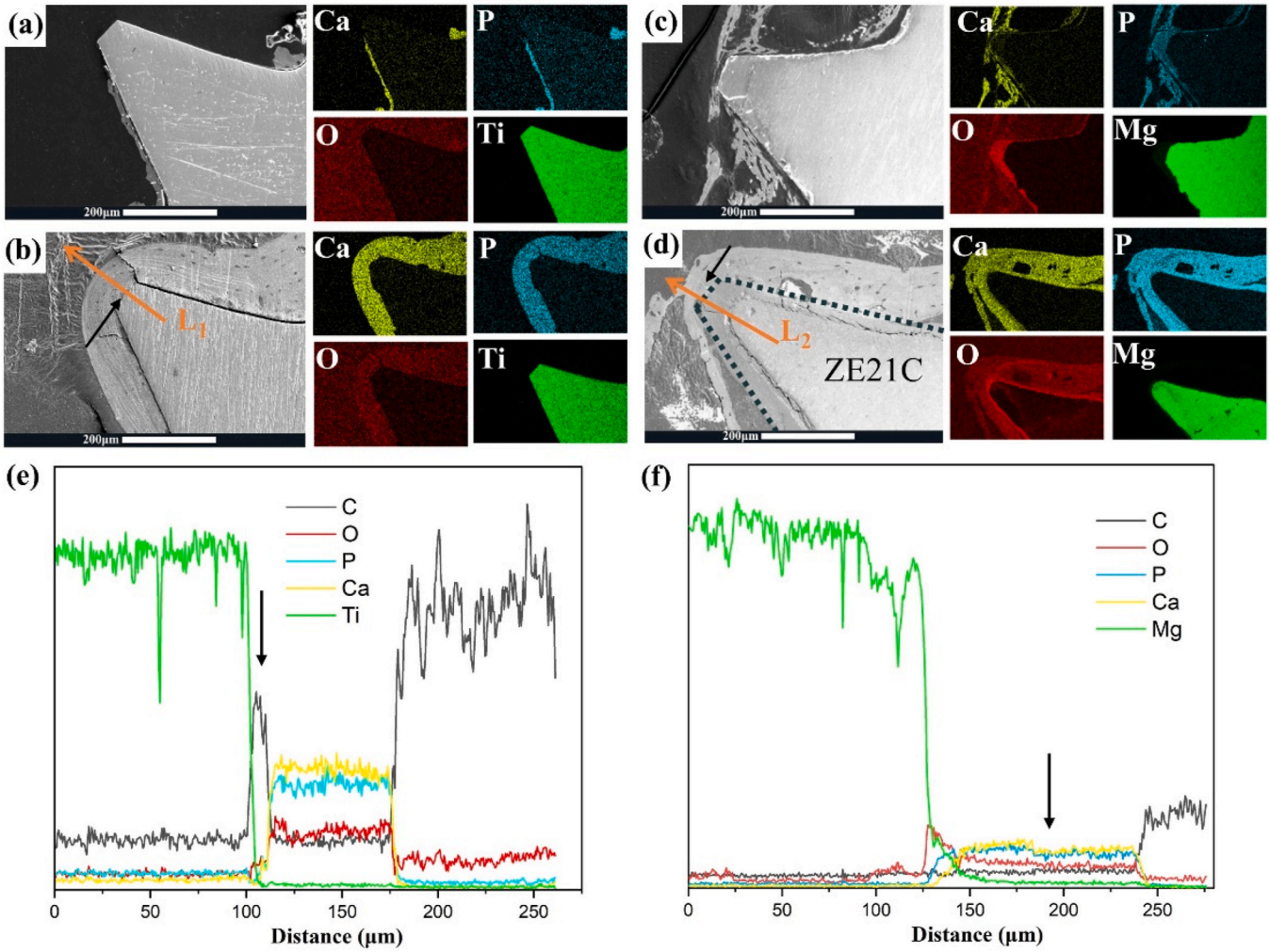

Fig. 7. SEM images and surface scan element distribution of the TC4 suture anchor threads at (a) 2 and (b) 12 weeks post-implantation. SEM images and surface scan element distribution of the ZE21C anchor threads at (c) 2 and (d) 12 weeks post-implantation. (e) L_1 line scan element distribution. (f) L_2 line scan element distribution. Black arrow: implant-bone interface.

magnesium alloy anchor had a better osteoconductive effect to enhance the bone formation.

3.5. Bone healing above the suture anchor

According to the representative 2D and 3D reconstructed images of the bone tissue above the suture anchor in the ZE21C group, it can be observed that the volume of bone tissue increased, and its integration with head of the suture anchor became more tight throughout the implantation period (Fig. 8a). The trabecular bone parameters (bone volume vs. total volume [BV/TV], trabecula number [Tb. N], trabecula thickness [Tb. Th], and trabecula separation [Tb. Sp]) were also measured, as shown in Fig. 8b. At 2, 4, 8, and 12 weeks, the BV/TV and TN of the ZE21C group were significantly higher than those of the TC4 group, while the Tb. Sp was lower than that of the control group. The Tb. Th of the ZE21C group was higher than the TC4 group at 2 and 4 weeks after surgery but became lower than the TC4 group at 8 and 12 weeks after surgery.

3.6. Knee ROM results

All the rats returned to normal activity without lameness or abnormality at two weeks after surgery. The knee ROM values are shown in Fig. 9. Within the first four weeks, the knee ROM in both groups was low and kept at about 90°, which may be due to ligament swelling limiting joint activity. At eight weeks after surgery, knee ROM was significantly improved in the two groups, at 103.11 ± 0.38° in the TC4 group and 104.44 ± 0.38° in the ZE21C group ($p < 0.05$). At 12 weeks post-operation, the knee ROM of the two groups returned similar to the normal level (110°–120°, marked in red dashed lines), at 113 ± 0.58° in the TC4 group and 115.44 ± 1.35° in the ZE21C group ($p < 0.05$).

3.7. Gross observation of the rat tibia

The general results of the gross observations are shown in Fig. 10. Two weeks after the operation, compared to the patellar ligament attached to the tibia only through the tensile force of anchors and sutures, there was much connective tissue in the repaired parts of the ZE21C and TC4 groups. Moreover, the patellar ligaments were swollen, but there were no other problems, such as rupture or pus. Four weeks after surgery, small fibrovascular vessels appeared in the bone-ligament interface. Eight weeks after surgery, a large number of fibrous blood vessels can be observed at the interface. At 12 weeks after surgery, the bone-ligament interface is already well integrated, fibrous blood vessels are well-distributed throughout the ligament and the interface, and the toughness is good. Overall, there were no significant differences between the ZE21C and the TC4 groups.

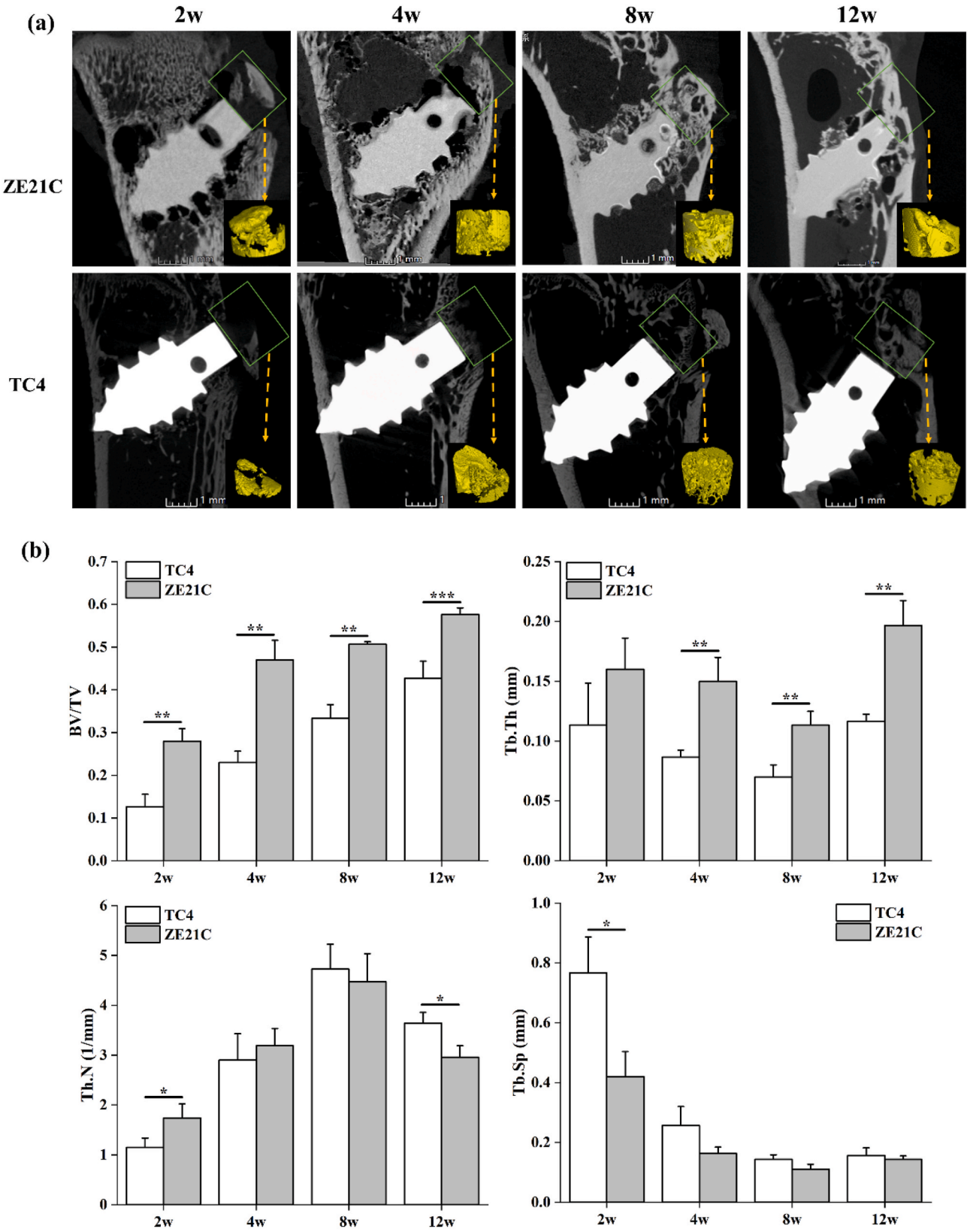

Fig. 8. Micro-CT analysis of the suture anchor and bone mass above the suture anchor. (a) Representative 2D Micro-CT images of the tibias with suture anchors at 2, 4, 8, and 12 weeks post-surgery and 3D reconstructed models of the bone above the suture anchor. Green boxes indicate the region of interest. (b) The parameters of bone trabecular structure (BV/TV, Tb. N, Tb. Th, and Tb. Sp) above the suture anchor within 12 weeks after the operation (n = 3). Data are presented as the mean ± SD. $^{*}p < 0.05$, $^{**}p < 0.01$, $^{***}p < 0.001$.

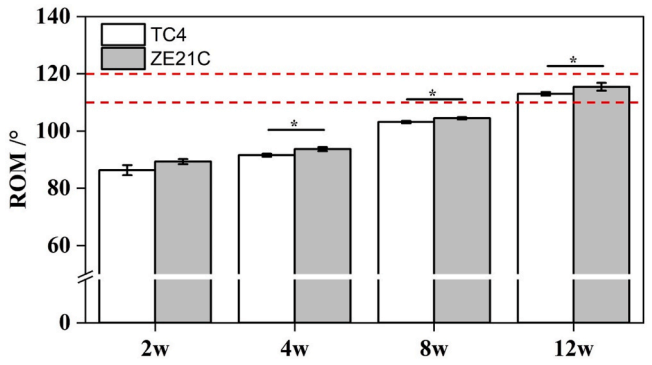

Fig. 9. Maximum ROM of the rat knee in two groups. Red dashed lines represent the normal range (110°–120°). *$p < 0.05$.

3.8. Histological analysis

The results of HE staining are shown in Fig. 11. At 4 weeks after surgery, inflammatory cells were observed at the ligament-bone interface in the two groups. The new bone trabecular space above the suture anchor was larger, and its combination with the ligament was loosen. At 8 weeks after the surgery, the number of inflammatory cells in the ligament-bone interface was significantly reduced in both groups, while the number of fibroblasts was significantly increased. Mutual growth also occurred between ligament and bone. Moreover, the above phenomenon was more obvious in the ZE21C group than in the control group. At 12 weeks after surgery, the ligament-bone junction tissue connection in the ZE21C group was more compact than that in the TC4 group and had less scar tissue.

The results of safranin O & fast green and toluidine blue staining are shown in Fig. 12. In the ZE21C group, fibrocartilage regeneration was observed at 4 weeks after surgery. In contrast, only fibrovascular granulation tissue was observed in the TC4 group. There was more newly formed fibrocartilage at 8 weeks after surgery, while it could be seen that the fibrocartilage zone in the ZE21C group was larger and in an orderly arrangement than TC4 group. At 12 weeks after surgery, the ZE21C group had more mature fibrocartilage tissue and a much larger tissue area than the control group.

3.9. Blood indices results

Whole blood metallic elements of Mg, Zn, Y, Nd and Zr of samples collected at 12 weeks after surgery showed no significant difference between ZE21C group and TC4 group (Table 3). There was also no significant difference in liver and kidney functions between two groups (Table 4). These results suggested the implantation of ZE21C suture anchor didn't cause metabolism disorder of Mg, Zn, Y, Nd and Zr alloying elements and disorder of liver and kidney function.

3.10. Biomechanical testing results

The results of biomechanical test are shown in Fig. 13c–d. It showed ruptures at the ligament-bone junction and the suture anchors wasn't pulled out. From Fig. 13g–f, at two weeks after surgery, the ultimate failure load of the ZE21C group was 140.3% higher than that of the TC4 group ($p < 0.05$), and its tensile strength and stiffness were 146.5% and 164.6% higher than those of the TC4 group, respectively ($p < 0.01$). At four weeks after surgery, the ultimate failure load and tensile strength of the ZE21C group were 43.4% and 70.4% higher than those of the TC4 group, respectively ($p < 0.05$). The stiffness of the ZE21C group was 39.8% higher than that of the TC4 group, but no statistical significance was detected. At eight weeks after surgery, the ultimate failure load and stiffness of the ZE21C group were 31.2% and 33.2% higher than those of the TC4 group, respectively ($p < 0.05$). At the same time, the tensile strength was 36.3% higher than the control group, but it was not statistically significant. At 12 weeks after surgery, the ultimate failure load and tensile strength of the ZE21C group were 22.9% and 13.8% higher than those of the TC4 group, respectively ($p < 0.01$), while the stiffness was 38.8% higher than that of the TC4 group, but no statistical significance was detected.

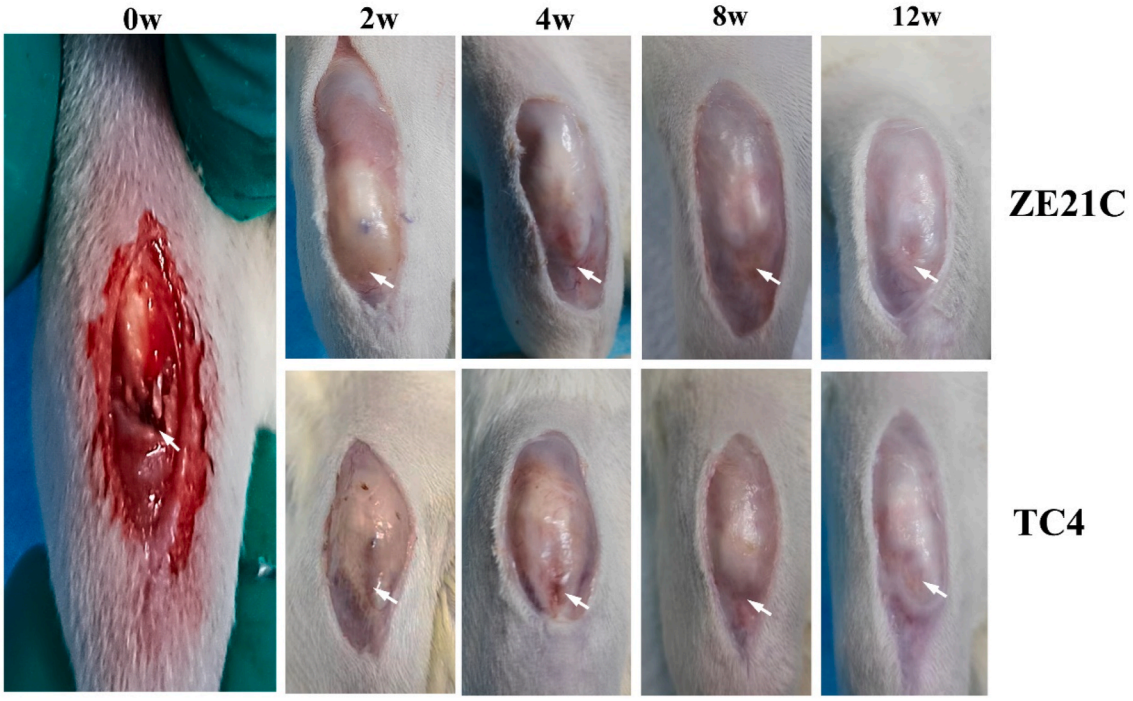

Fig. 10. Photos of patellar ligament-tibia reconstruction at 0, 2, 4, 8, and 12 weeks post-operation. White arrows, Repair site.

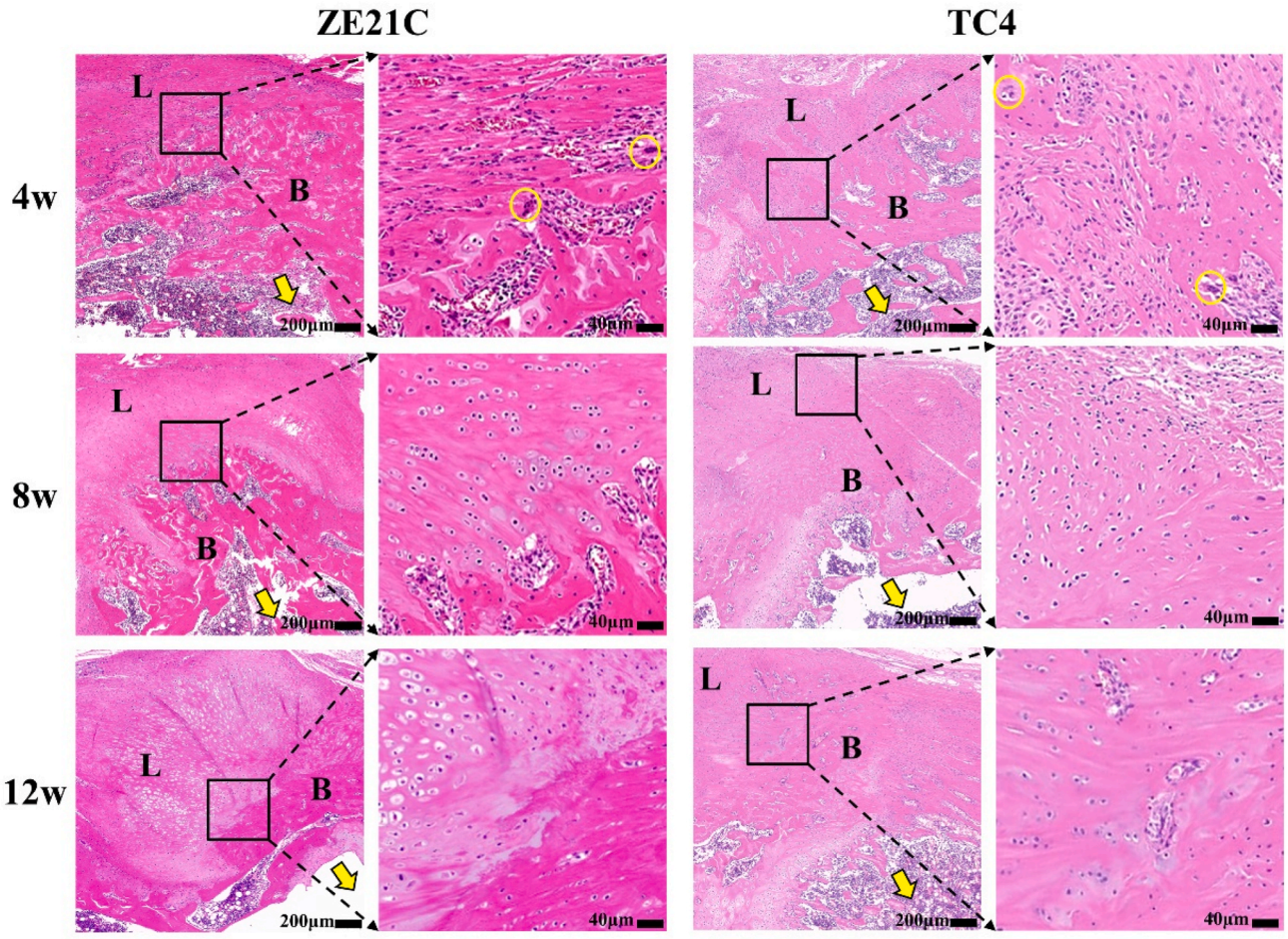

Fig. 11. HE staining results of the ligament-bone interface after suture anchor implantation in SD rats for 4, 8, and 12 weeks. Yellow arrows, suture anchor insertion location; yellow circles, inflammatory cells. L: Ligament, B: Bone.

4. Discussion

In this study, patellar ligament-tibia reconstruction model in SD rats was used to study the degradation behavior and reparative effect of the ZE21C suture anchor. The radiological, histological, and biomechanical results showed that the ZE21C suture anchor degraded gradually *in vivo*, maintained structural integrity within 12 weeks of implantation and promoted ligament-bone healing.

The degradation of magnesium alloy implants will inevitably generate hydrogen, and the generation and absorption of hydrogen have been the focus of contemporary researchers [16,20,21]. Here, we reported that hydrogen was present in the subcutaneous position in the ZE21C group one day after implantation, which might be due to a gap between the ligament and bone after surgery. Two weeks after surgery, the subcutaneous emphysema was absorbed as the gap closed, and released hydrogen only appeared around the ZE21C suture anchor. Furthermore, as the implantation time went on, the amount of hydrogen accumulated gradually decreased until it disappeared, consistent with the gradual decreasing trend of the degradation rate shown in Fig. 6b. Wang et al. [21] also reported that gas generation was observed in magnesium alloy implants at two weeks, and then the gas disappeared after two months. It is believed that the released gas was continuously absorbed by the surrounding tissue. Moreover, gas generation did not interfere with the osseointegration around the magnesium alloy anchor and the growth of the bone tissue above the suture anchor (Figs. 7 and 8). These results were similar to the study by N. G. Grun et al. [29], who implanted magnesium nails in sheep and rats to observe the gas effect and reported gas release in these animal models without interfering with bone formation or growth.

D. Ntalos et al. [30] found that the pull-out strength of the suture anchor was strongly correlated with the thickness of the surrounding cortical bone. J. G. Kim et al. [31] significantly improved bone formation above the suture anchor by applying BMP-2, which helped restore biomechanical strength between the bone and the ligament. It can also be seen that the quality of cortical bone healing above the suture anchor was an important factor for measuring performance of suture anchor. In our current research, bone regeneration was main within four weeks. From 4 to 8 weeks after surgery, the regenerated bone gradually transformed into mature bone tissue. From 8 to 12 weeks after surgery, the braided bone gradually formed lamellar bone (Figs. 8 and 11), and these results were consistent with the normal cortical bone defect repair process [32]. According to the trabecular bone parameters obtained, we found that the volume of bone tissue above the ZE21C suture anchor was significantly higher than that of the control group. Moreover, trabecular bone thickness and separation in the ZE21C group were also better than that in the control group. These results indicated that the ZE21C magnesium alloy suture anchor not only promoted the bone regeneration above the suture anchor but also improved the quality of the regenerated bone [17]. Furthermore, although the number of trabecular bones of ZE21C group was lower than that of the control group, the thickness of cortical bone was higher than that of the control group at eight weeks (Fig. 8b), which indicates that formation of lamellar bone above the ZE21C suture anchor was earlier than control group [33]. This might be because the Mg^{2+} released during the degradation of the ZE21C suture anchor promoted braided bone to form lamellar bone above the suture anchor [19].

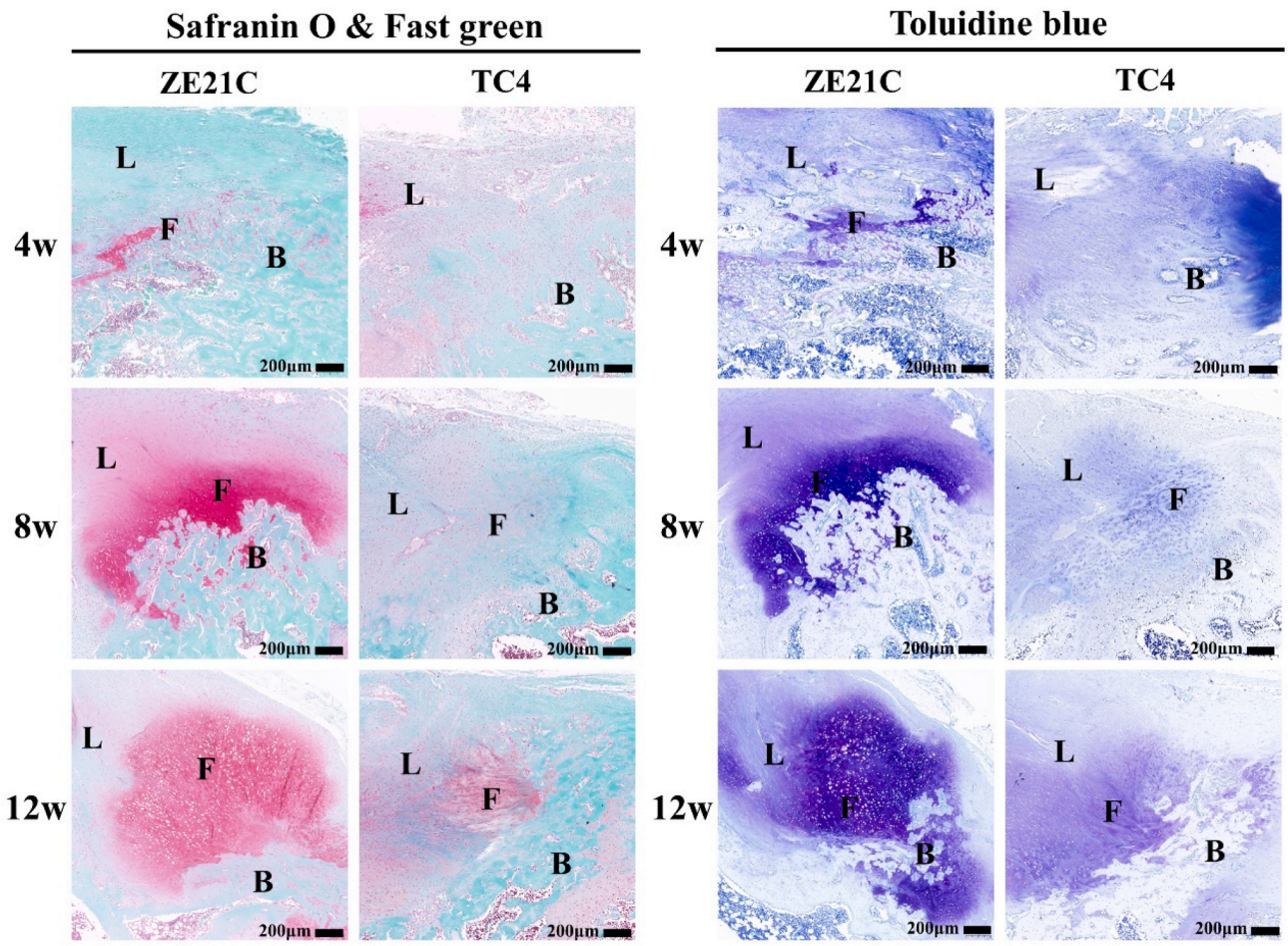

Fig. 12. Safranin O & Fast green and toluidine blue staining results of the ligament-bone interface after suture anchor implantation in SD rats for 4, 8, and 12 weeks. L: Ligament, F: Fibrocartilage, B: Bone.

Table 3
Comparison of whole blood elements of Mg, Zn, Y, Nd and Zr between two groups of rats at 12 weeks after surgery. Undetected refers to detected content <0. 01 μg/L.

Group	Mg (mg/L)	Zn (mg/L)	Y (μg/L)	Nd(μg/L)	Zr(μg/L)
ZE21C	38.67 ± 4.88	4.10 ± 0.22	Undetected	4.54 ± 1.22	14.36 ± 4.21
TC4	33.83 ± 2.18	3.75 ± 0.26	Undetected	3.50 ± 0.14	7.74 ± 0.50
P	0.193	0.146	0.123	0.524	0.054

Table 4
Comparison of liver and kidney function indexes between two groups of rats at 12 weeks after surgery.

Group	Aspartate aminotransferase (U/L)	Serum albumin (g/L)	Serum creatinine (μmol/L)	Urea nitrogen (mmol/L)
ZE21C	145.43 ± 30.35	33.57 ± 3.41	47.67 ± 5.80	6.36 ± 0.68
TC4	178.07 ± 36.82	32.03 ± 1.48	45.13 ± 2.44	7.13 ± 0.36
P	0.302	0.514	0.159	0.524
Normal	69.7–322.9	31.7–43.7	19.43–64.97	2.08–7.75

An ideal biodegradable implant should have an appropriate degradation rate to ensure that it can maintain its mechanical integrity during the healing process, withstand loads, gradually degrade, and then eventually be fully resorbed [34]. From the *in vitro* experiments, we found that the ZE21C suture anchor degraded slowly, and beneficial calcium and phosphorus products generated and accumulated on its surface. Moreover, the degradation of magnesium alloy implant was not only related to the stress it was subjected to, but also the condition of implant location [35,36]. Combining the results of the finite element and vivo degradation (Figs. 2 and 6), the most severely degraded part was the tail of the suture anchor in high stress concentration within 4 weeks after surgery. After the degradation of the tip, the degradation of the anchor tail gradually slowed down, indicating that the high stress concentration part of mg-based suture anchor will degrade rapidly in early implantation period [19]. Although there was stress concentration in the head of suture anchor, the small stress concentration had little influence on the degradation. In contrast, the small stress distribution in the middle of the anchor was uniform and wrapped by the surrounding tissue, resulting in uniform degradation. However, the head of ZE21C suture anchor showed local degradation at four weeks after surgery. This may be because the bone regeneration and bone transform above the suture anchor accelerated vascularization and fluid exchange , which resulted in faster degradation of the surrounding magnesium alloy implants [37]. Although the local degradation of the anchor head in the later stages may affect the mechanical properties, the accelerated healing of the bone tissue above the suture anchor will reduce the required mechanical properties of the suture anchor [31]. Therefore, the deterioration manner in the mechanical integrity of ZE21C suture anchors may well match ligament-bone junction healing process without fixation concerns.

In this study, we also investigated the reparative effect of ZE21C

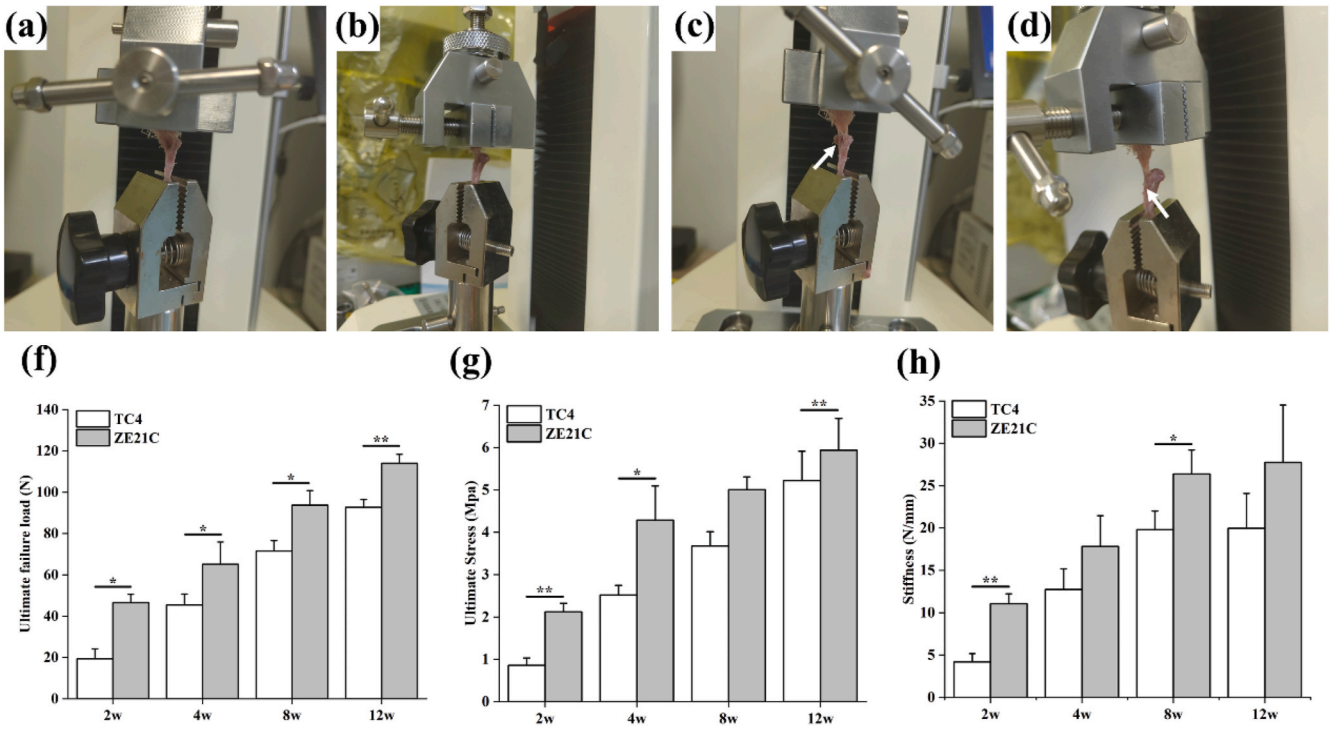

Fig. 13. Photos of the biomechanical test: (a) front view, (b) side view. Photos of the rupture of the ligament and bone: (c) front view, (d) side view. (e) Ultimate failure load, (f) ultimate stress, and (g) stiffness results after suture anchor implantation in SD rats for 2, 4, 8, and 12 weeks. White arrows: rupture site. Data are presented as the mean ± SD. $^{*}p < 0.05$, $^{**}p < 0.01$, $^{***}p < 0.001$.

suture anchor on ligament-bone junction. The histological results showed that the ZE21C suture anchor had more mature fibrocartilage tissue and less scar tissue compared with the TC4 group, indicating that ZE21C suture anchor can promote ligament integration into bone after reconstruction. Our histological finding was comparable to the observation by B. Chen et al. [38], who demonstrated that the sustained released Mg^{2+} in situ greatly promoted fibrocartilage formation. It is generally accepted that the long-term goal of ligament-bone reconstruction is to obtain biological union at the attachment site of the ligament and restore a highly ordered attachment point, which will allow for firm attachment of the reconstruction site [18,39]. Here, the biomechanical results show that the ultimate failure load, ultimate stress, and stiffness of the ZE21C group are significantly higher than those of TC4 group. Wang et al. [40] observed that Mg-pretreated periosteum promoted the bony ingrowth and peri-tunnel bone formation at the tendon-bone interface in rabbits with ACL reconstruction, which leading to a significant increase in the bonding strength between the tendon graft and the bone tunnel. Hence, it indicated that the superior biomechanics strength in ZE21C group is not only related to better bone healing above the suture anchor but also attributed to more fibrocartilaginous interface regeneration. In summary, ZE21C group exhibited superior results which might be ascribed to Mg^{2+} released from the corroded ZE21C suture anchor having the beneficial effects on ligament-bone junction healing.

The present study has some limitations. Although the designed suture anchor can be implanted in the rat tibia, the size of animal was small. In the future, experiments on larger animals may be considered to verify the effectiveness of this new magnesium alloy suture anchor. In addition, with the continuous application of finite element technology to various biomechanical experiments [41,42], we will optimize the structure of magnesium alloy suture anchor to enhance its initial mechanical properties and avoid rapid stress corrosion using finite element method.

5. Conclusion

In this paper, ZE21C magnesium alloy was used to prepare suture anchors for reconstructing the patellar ligament and proximal tibia in SD rats. The ZE21C suture anchor could maintain its mechanical structure within 12 weeks of implantation. The tail of the suture anchor in high stress concentration degraded rapidly during the early implantation stage, while bone healing above anchor in the late implantation stage accelerated the degradation of the anchor head. Furthermore, the ZE21C suture anchor can promote the repair of the ligament-bone through promoting bone healing above the suture anchor and fibrocartilaginous interface regeneration. This study provided data and theoretical guidance for the clinical application of degradable magnesium alloy suture anchors in the future.

Ethics approval and consent to participate

In this study, we cooperated with the Zhengzhou orthopedic hospital in China to complete the patellar ligament-proximal tibia reconstruction surgery. The animal experiments for patellar ligament-proximal tibia reconstruction were authorized by the Ethics Committee of the Animal Experimental Center of Zhengzhou University (License No. SYXK(Yu) 2020-0008).

CRediT authorship contribution statement

Delin Ma: Data curation, Conceptualization, Methodology, Formal analysis, Writing – original draft. **Jun Wang:** Data curation, Investigation, Writing – review & editing, Methodology. **Mingran Zheng:** Supervision. **Yuan Zhang:** Data curation, Investigation. **Junfei Huang:** technology support, Formal analysis. **Wenxiang Li:** Investigation, Formal analysis. **Yiwen Ding:** Investigation. **Yunhao Zhang:** Investigation, Formal analysis. **Shijie Zhu:** Resources, Methodology. **Liguo Wang:** Conceptualization, Funding acquisition. **Xiaochao Wu:** Conceptualization, Writing – review & editing. **Shaokang Guan:**

Conceptualization, Visualization, Funding acquisition, Funding acquisition, Writing – review & editing.

Declaration of competing interest

No potential conflict of interest was reported by the authors.

Acknowledgments

This work was supported by Scientific and Technological Project in Henan Province (212102310236, 202102210015), National Natural Science Foundation of China (51701184, 51671175), the Key Projects of the Joint Fund of the National Natural Science Foundation of China (U1804251), and the Postgraduate Independent Innovation Project of Zhengzhou University (20211203). We thank Taohong Huang at Shimadzu (China) Co., Ltd. For the help of technology and equipment of Micro-CT.

References

[1] W.L. Lim, L.L. Liau, M.H. Ng, S.R. Chowdhury, J.X. Law, Current progress in tendon and ligament tissue engineering, Tissue Eng. Regen. Med. 16 (6) (2019) 549–571.
[2] N.L. Leong, J.L. Kator, T.L. Clemens, A. James, M. Enamoto-Iwamoto, J. Jiang, Tendon and ligament healing and current approaches to tendon and ligament regeneration, J. Orthop. Res. 38 (1) (2020) 7–12.
[3] P. Behrendt, T. Kluter, A. Seekamp, Injuries of major tendons : review of current diagnostic and surgical standards, Chirurg. 88 (2) (2017) 175–186.
[4] F. Migliorini, A. Baroncini, J. Eschweiler, M. Tingart, N. Maffulli, Interference screws vs. suture anchors for isolated medial patellofemoral ligament femoral fixation: a systematic review, J. Sport. Health Sci. 11 (1) (2022) 123–129.
[5] S. Chaudhry, K. Dehne, F. Hussain, A review of suture anchors, J. Orthop. Traumatol. 33 (4) (2019) 263–270.
[6] L.E. Visscher, C. Jeffery, T. Gilmour, L. Anderson, G. Couzens, The history of suture anchors in orthopaedic surgery, Clin. Biomech. 61 (2019) 70–78.
[7] Y.G. Kang, J.H. Kim, J.W. Shin, J.M. Baik, H.J. Choo, Induction of bone ingrowth with a micropore bioabsorbable suture anchor in rotator cuff tear: an experimental study in a rabbit model, J. Shoulder Elbow Surg. 22 (11) (2013) 1558–1566.
[8] C.C. Tai, H.L. Lo, C.K. Liaw, Y.M. Huang, Y.H. Huang, K.Y. Yang, C.C. Huang, S. I. Huang, H.H. Shen, T.H. Lin, C.K. Lu, W.C. Liu, J.S. Sun, P.I. Tsai, C.Y. Chen, Biocompatibility and biological performance evaluation of additive-manufactured bioabsorbable iron-based porous suture anchor in a rabbit model, Int. J. Mol. Sci. 22 (14) (2021).
[9] C.H. Cho, K.C. Bae, D.H. Kim, Biomaterials used for suture anchors in orthopedic surgery, Clin. Orthop. Surg. 13 (3) (2021) 287–292.
[10] T.K. Kaar, R.C. Schenck, M.A. Wirth Jr., C.A. Rockwood Jr., Complications of metallic suture anchors in shoulder surgery: a report of 8 cases, Arthroscopy. 17 (1) (2001) 31–37.
[11] D.J. Scholten 2nd, B.R. Waterman, Editorial commentary: taking a "PEEK" at suture anchor composition following arthroscopic rotator cuff repair: is bio really better? Arthroscopy. 36 (2) (2020) 397–399.
[12] K. Ro, S. Pancholi, H.S. Son, Y.G. Rhee, Perianchor cyst formation after arthroscopic rotator cuff repair using all-suture-type, bioabsorbable-type, and PEEK-type anchors, Arthroscopy 35 (8) (2019) 2284–2292.
[13] J.K. Khoo, J.H.T. Lee, P.H. Lam, A.Q. Wei, J. Ronquillo, G.A.C. Murrell, Cytotoxicity and biomechanics of suture anchors used in labral repairs, JSES Open Access 3 (1) (2019) 29–36.
[14] S.H. Kim, D.Y. Kim, J.E. Kwon, J.S. Park, J.H. Oh, Perianchor cyst formation around biocomposite biodegradable suture anchors after rotator cuff repair, Am. J. Sports Med. 43 (12) (2015) 2907–2912.
[15] D. Zhao, F. Witte, F. Lu, J. Wang, J. Li, L. Qin, Current status on clinical applications of magnesium-based orthopaedic implants: a review from clinical translational perspective, Biomaterials 112 (2017) 287–302.
[16] J.L. Wang, J.K. Xu, C. Hopkins, D.H. Chow, L. Qin, Biodegradable magnesium-based implants in orthopedics-A general review and perspectives, Adv. Sci. 7 (8) (2020), 1902443.
[17] D.H.K. Chow, J. Wang, P. Wan, L. Zheng, M.T.Y. Ong, L. Huang, W. Tong, L. Tan, K. Yang, L. Qin, Biodegradable magnesium pins enhanced the healing of transverse patellar fracture in rabbits, Bioact. Mater. 6 (11) (2021) 4176–4185.
[18] J. Wang, J. Xu, W. Fu, W. Cheng, K. Chan, P.S. Yung, L. Qin, Biodegradable magnesium screws accelerate fibrous tissue mineralization at the tendon-bone insertion in anterior cruciate ligament reconstruction model of rabbit, Sci. Rep. 7 (2017), 40369.
[19] S. Huang, B. Wang, X. Zhang, F. Lu, Z. Wang, S. Tian, D. Li, J. Yang, F. Cao, L. Cheng, Z. Gao, Y. Li, K. Qin, D. Zhao, High-purity weight-bearing magnesium screw: translational application in the healing of femoral neck fracture, Biomaterials. 238 (2020), 119829.
[20] H. Zhou, B. Liang, H. Jiang, Z. Deng, K. Yu, Magnesium-based biomaterials as emerging agents for bone repair and regeneration: from mechanism to application, J. Magnesium. Alloy. 9 (3) (2021) 779–804.
[21] J. Wang, H. Jiang, Y. Bi, J. Sun, M. Chen, D. Liu, Effects of gas produced by degradation of Mg-Zn-Zr Alloy on cancellous bone tissue, Mater Sci. Eng. C Mater. Biol. Appl. 55 (2015) 556–561.
[22] Y. Huang, F. Hung, F. Kuan, K. Hsu, W. Su, C. Li, Microstructure, mechanical properties, degradation behavior, and implant testing of hot-rolled biodegradable ZKX500 magnesium alloy, Appl. Sci. 11 (22) (2021).
[23] Y. Xu, J. Li, M. Qi, J. Gu, Y. Zhang, Effect of extrusion on the microstructure and corrosion behaviors of biodegradable Mg–Zn–Y–Gd–Zr alloy, J. Mater. Sci. 55 (3) (2019) 1231–1245.
[24] Y. Yang, C. Lu, L. Shen, Z. Zhao, S. Peng, C. Shuai, In-situ deposition of apatite layer to protect Mg-based composite fabricated via laser additive manufacturing, J. Magnesium. Alloy. (2021), https://doi.org/10.1016/j.jma.2021.04.009.
[25] X. Song, L. Chang, J. Wang, S. Zhu, L. Wang, K. Feng, Y. Luo, S. Guan, Investigation on the in vitro cytocompatibility of Mg-Zn-Y-Nd-Zr alloys as degradable orthopaedic implant materials, J. Mater. Sci. Mater. Med. 29 (4) (2018) 44.
[26] H. Sano, A. Takahashi, D. Chiba, T. Hatta, N. Yamamoto, E. Itoi, Stress distribution inside bone after suture anchor insertion: simulation using a three-dimensional finite element method, Knee Surg. Sports Traumatol. Arthrosc. 21 (8) (2013) 1777–1782.
[27] M. Tanvir, L. Irène, V. Isabelle, Experimental and finite element analyses of bone strains in the growing rat tibia induced by in vivo axial compression, Journal of the Mechanical Behavior of Biomedical Materials 94 (2019) 176–185.
[28] W. Peng, J. Chen, X. Shan, Y. Wang, F. He, X. Wang, L. Tan, K. Yang, Mg-based absorbable membrane for guided bone regeneration (GBR): a pilot study, Rare Met. 38 (6) (2019) 577–587.
[29] N.G. Grun, P. Holweg, S. Tangl, J. Eichler, L. Berger, J. van den Beucken, J. F. Loffler, T. Klestil, A.M. Weinberg, Comparison of a resorbable magnesium implant in small and large growing-animal models, Acta Biomater. 78 (2018) 378–386.
[30] D. Ntalos, G. Huber, K. Sellenschloh, H. Saito, K. Puschel, M.M. Morlock, K. H. Frosch, T.O. Klatte, All-suture anchor pullout results in decreased bone damage and depends on cortical thickness, Knee Surg. Sports Traumatol. Arthrosc. 29 (7) (2021) 2212–2219.
[31] J.G. Kim, H.J. Kim, S.E. Kim, J.H. Bae, Y.J. Ko, J.H. Park, Enhancement of tendon-bone healing with the use of bone morphogenetic protein-2 inserted into the suture anchor hole in a rabbit patellar tendon model, Cytotherapy. 16 (6) (2014) 857–867.
[32] R. Ye, X. Zhang, H. Yan, Y. Pan, N. Huang, L. Lu, Z. Jiang, Poly(3-hydroxybutyrate-co-3-hydroxyvalerate) nanofibers for repairing rabbit bone defects, Chin J. Tissue Eng. Res. 16 (34) (2012).
[33] H. Lu, C. Zheng, Z. Wang, C. Chen, H. Chen, J. Hu, Effects of low-intensity pulsed ultrasound on new trabecular bone during bone-tendon junction healing in a rabbit model: a synchrotron radiation micro-CT study, PLoS One 10 (4) (2015), e0124724.
[34] J. Niu, M. Xiong, X. Guan, J. Zhang, H. Huang, J. Pei, G. Yuan, The in vivo degradation and bone-implant interface of Mg-Nd-Zn-Zr alloy screws: 18 months post-operation results, Corrosion Sci. 113 (2016) 183–187.
[35] P. Sekar, N. S, V. Desai, Recent progress in in vivo studies and clinical applications of magnesium based biodegradable implants – a review, J. Magnesium. Alloy. 9 (4) (2021) 1147–1163.
[36] Y.T. Chen, F.Y. Hung, Y.L. Lin, C.Y. Lin, Biodegradation ZK50 magnesium alloy compression screws: mechanical properties, biodegradable characteristics and implant test, J. Orthop. Sci. 25 (6) (2020) 1107–1115.
[37] D. Kruger, S. Galli, B. Zeller-Plumhoff, D.C.F. Wieland, N. Peruzzi, B. Wiese, P. Heuser, J. Moosmann, A. Wennerberg, R. Willumeit-Romer, High-resolution ex vivo analysis of the degradation and osseointegration of Mg-xGd implant screws in 3D, Bioact Mater 13 (2022) 37–52.
[38] B. Chen, Y. Liang, L. Bai, M. Xu, J. Zhang, B. Guo, Z. Yin, Sustained release of magnesium ions mediated by injectable self-healing adhesive hydrogel promotes fibrocartilaginous interface regeneration in the rabbit rotator cuff tear model, Chem. Eng. J. 396 (2020).
[39] P. Cheng, P. Han, C. Zhao, S. Zhang, H. Wu, J. Ni, P. Hou, Y. Zhang, J. Liu, H. Xu, S. Liu, X. Zhang, Y. Zheng, Y. Chai, High-purity magnesium interference screws promote fibrocartilaginous entheses regeneration in the anterior cruciate ligament reconstruction rabbit model via accumulation of BMP-2 and VEGF, Biomaterials. 81 (2016) 14–26.
[40] J. Wang, J. Xu, X. Wang, L. Sheng, L. Zheng, B. Song, G. Wu, R. Zhang, H. Yao, N. Zheng, M.T. Yun Ong, P.S. Yung, L. Qin, Magnesium-pretreated periosteum for promoting bone-tendon healing after anterior cruciate ligament reconstruction, Biomaterials. 268 (2021), 120576.
[41] H. Sano, K. Imagawa, N. Yamamoto, H. Ozawa, A.T. Yokobori, E. Itoi, Predicting failures of suture anchors used for rotator cuff repair: a CT-based 3-dimensional finite element analysis, Bio Med. Mater. Eng. 25 (4) (2015) 371–380.
[42] T. Su, H. Tang, J. Jang, C. Chen, H. Chen, Design and development of magnesium-based suture anchor for rotator cuff repair using finite element analysis and in vitro testing, Appl. Sci. 11 (20) (2021).